JOURNAL OF SOLID STATE CHEMISTRY 88, 291–302 (1990)

Phase Equilibrium Study of the Y–Ba–Ni–O System and Structural Characterization of the New Quasi-One-Dimensional Oxide Y_2BaNiO_5

D. J. BUTTREY[1] AND J. D. SULLIVAN

Department of Chemical Engineering, University of Delaware, Newark, Delaware 19716

AND A. L. RHEINGOLD

Department of Chemistry, University of Delaware, Newark, Delaware 19716

Received May 1, 1990

DEDICATED TO J. M. HONIG ON THE OCCASION OF HIS 65TH BIRTHDAY

Phase equilibria in the Y_2O_3–BaO–NiO system were studied in the temperature range 1000–1350°C in air. In addition to previously reported compositions, the new phase Y_2BaNiO_5 was identified. Conditions for synthesis and stability of Y_2BaNiO_5 are reported, as well as the dependence of oxygen nonstoichiometry and lattice parameters on conditions of preparation. Single crystals were obtained by rf induction melting and the structure was refined by four circle X-ray diffraction. Y_2BaNiO_5 is isomorphous with Nd_2BaNiO_5 and consists of isolated, highly compressed chains of corner-shared NiO_6 octahedra.

Introduction

Phase equilibria in ternary and higher-order copper oxide systems have been the subject of intense investigation over the past few years as a consequence of the immense interest in high-temperature superconductivity. The corresponding phase diagrams of systems containing other first-row transition metals, however, remain less well characterized. The objective of this investigation was to examine phase behavior in the Y–Ba–Ni–O system and identify and characterize possible low-dimensional phases. To the best of our knowledge, no previous reports on this quarternary system have appeared in the literature; however, each of the respective ternary oxide systems have been investigated.

The Y–Ni–O system is known to contain no ternary phases with divalent nickel (*1*). Preparation of the trivalent nickel-containing phase, $YNiO_3$, by direct combination of NiO and Y_2O_3 under 400 atm O_2 at 1000°C has been reported by Arjomand and Machin (*2*).

The Y–Ba–O system is somewhat complex, containing a number of ternary phases which are stable in air. Muller-Buschbaum (*3*) first identified the compound Y_2BaO_4, but did not report any structural data. Y_2BaO_4 and $Y_4Ba_3O_9$ were later reported by

[1] To whom correspondence should be addressed.

0022-4596/90 $3.00

Maister and Lopato (*4*) in a study in which phases of these stoichiometries were also shown to exist for all lanthanide barium oxides. Lopato *et al.* (*5*) also reported a complete phase diagram of the Y_2O_3–BaO binary above 1200°C. They concluded that Y_2BaO_4 is stable below 1400°C and that $Y_4Ba_3O_9$ is stable up to the congruent melting point at 2160°C. Further investigation of Y_2O_3–BaO by Kwestroo *et al.* (*6*) revealed additional phases that only exist below 1200°C. Along with the two end members, $Y_2Ba_4O_7$, $Y_4Ba_3O_9$, $Y_2Ba_2O_5$, and Y_2BaO_4 were reported to be stable in dry air. $Y_2Ba_4O_7$ is phase pure at 1000°C, but decomposes above 1100°C. The unit cell of this tetragonal compound has subsequently been indexed by Kovba *et al.* (*7*). The study by Kwestroo *et al.* (*6*) also reported that $Y_2Ba_2O_5$ is tetragonal and decomposes above 1000°C, but they were unable to synthesize the compound phase pure. Their investigation confirmed the previous work on the temperature ranges of stability of $Y_4Ba_3O_9$ and Y_2BaO_4, although slightly different unit cell parameters and symmetries were reported. More recently, the compound $Y_4Ba_3O_9$ has been reindexed in the hexagonal system by Wong-Ng *et al.* (*8*).

The Ba–Ni–O system has been reported by Lander (*9*) to contain the divalent nickel phases Ba_3NiO_4 and $BaNiO_2$. $BaNiO_2$ is described as black in appearance, stable in air, orthorhombic, and melting at 1240°C. In a later report, Lander (*10*) characterized the structure of $BaNiO_2$ as consisting of Ni^{2+} in square planar oxygen coordination, and having a paramagnetic moment of 1.83 μ_B, rather than the expected diamagnetic behavior for a square planar d^8 system. Krischner *et al.* (*11*) also reported an X-ray structural analysis of $BaNiO_2$, confirming the square planar arrangement of oxygen around Ni^{2+}. Krischner observed the expected diamagnetic susceptibility and attributed the apparent paramagnetic moment observed by Lander to the presence of a small amount of Ni^{3+} from nonstoichiometry. In contrast with both Lander's and Krischner's results, Arjomand and Machin (*2*) subsequently reported a paramagnetic moment of 3.14 μ_B for $BaNiO_2$. Ba_3NiO_4 is described as gray–green, unstable in air, hexagonal, and as having a melting point of 1160°C (*12*). Higher oxides of nickel with Ba/Ni = 1, such as $BaNiO_{2.36}$, $Ba_2Ni_2O_5$, and $BaNiO_3$, have also been reported (*2, 12–14*).

In the present investigation, we use X-ray ray diffraction to characterize the Y–Ba–Ni–O system in the temperature range 1000–1350°C in air. Under these conditions of synthesis, the oxidation state of nickel is expected to be predominantly divalent for all nickel-containing phases. A new phase, Y_2BaNiO_5, is identified and conditions for synthesis and stability are examined.

Experimental

The starting materials for all syntheses were Johnson–Matthey Grade 1 $BaCO_3$, Cerac 99.995% NiO, and Research Chemicals 99.99% Y_2O_3. For the phase diagram syntheses, 3- to 5-g mixtures of starting materials in nickel or alumina crucibles were ramped at 3°C/min from 1000 to 1200°C in a programmable 1700°C Lindberg box furnace. After allowing 1 hr to evolve moisture and decompose the carbonate, the temperature was ramped at 3°C/min to 1350°C and held for 6 hr to achieve substantial sintering. Samples were then cooled at 5°C/min to 1000°C, and subsequently quenched to room temperature. All syntheses were carried out in air. Single crystals were prepared by radio frequency skull melting as described in the next section.

X-ray powder diffraction data were obtained at 295 K with an automated Philips PW1710 diffractometer using Cu$K\alpha$ radiation (λ = 1.54060 Å) with a graphite monochromator on the detector arm. Single crystal X-ray diffraction was carried out on a

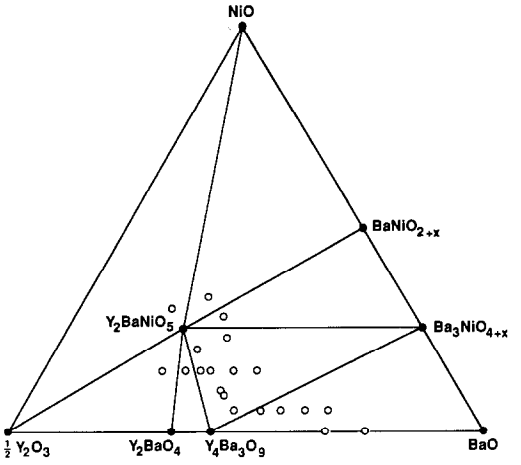

FIG. 1. The Y–Ba–Ni–O phase diagram in air in the temperature range 1000–1350°C. Open circles represent overall experimental compositions.

four-circle Nicolet $R3m/\mu$ diffractometer at 293 K using graphite-monochromated Mo$K\alpha$ radiation (λ = 0.71073 Å).

Controlled atmosphere anneals of Y_2BaNiO_5 were performed in a 1300°C Applied Test Systems tube furnace with appropriate research purity gases mixed with a Vacuum General Dynamass mass flow controller. Synthesis of 50 g of phase pure Y_2BaNiO_5 under the same conditions described for the phase diagram experiments provided the stock material for all anneals. The controlled oxygen fugacity anneals were monitored with an Y–ZrO_2 solid electrolyte cell calibrated against the Ni/NiO buffer. Low partial pressures of oxygen (10^{-5}–10^{-8} atm) were established using CO/CO_2 buffers, whereas mixtures of Ar/O_2 and CO_2/O_2 were used for more moderate oxygen pressures (10^3–1 atm). Appropriate flows of Ar, CO_2, and O_2 were mixed for the controlled carbon dioxide fugacity anneals. Samples were isothermally annealed for approximately 7 hr to avoid kinetic limitations on diffusion and/or reaction, and then were rapidly quenched to room temperature within the annealing atmosphere. The samples were immediately stored in mineral oil to prevent possible transfer of oxygen between sample and surroundings, although this does not appear to be a problem as stoichiometric crystals of Y_2BaNiO_5 show little evidence of acquiring measurable levels of excess oxygen as a result of exposure to air at room temperature.

The excess oxidation potential of the samples was determined by iodometric titrations with deaerated thiosulfate solutions in a nitrogen-filled glove box. The nominal concentrations of sodium thiosulfate solutions were optimized based on the anticipated level of nonstoichiometry in samples from each of the anneals. Standardization of the thiosulfate against primary standard arsenic sesquioxide was performed immediately prior to use. Blanks were also titrated, showing a negligible background correction in titrated volumes.

Results

The Y–Ba–Ni–O Phase Diagram

Phase equilibrium studies for the Y–Ba–Ni–O system in air between 1000 and 1350°C reveal the new phase Y_2BaNiO_5, as well as four other phases previously reported between the pure metal oxides. The phase diagram is presented in Fig. 1, with solid circles representing stable phases and open circles representing overall experimental compositions. The arrangement of Alkemade triangles shows that Y_2BaNiO_5 may exist in equilibrium with any of the phases in the ternary except BaO. Syntheses within the primary phase field of $BaNiO_{2+x}$ and Ba_3NiO_4 were avoided because the products were difficult to characterize, due to low melting points, tendency for hydration, and reaction with crucible materials.

$BaNiO_{2+x}$ was successfully prepared nearly phase pure in air at 1000°C, except for traces of unreacted material ($I/I_0 < 1\%$), by reaction in a crucible lined with oxidized Ni foil. X-ray powder diffraction data on

TABLE I

X-RAY POWDER DATA FOR HEXAGONAL $BaNiO_{2.36}$ WITH LATTICE PARAMETERS a = 5.706 AND c = 4.329 Å

$h\ k\ l$	d_{obsd} (Å)	d_{calcd} (Å)	I/I_o
100	4.97	4.94	1
101	3.259	3.256	35
110	2.853	2.853	100
200	2.471	2.471	5
002	2.166	2.165	5
201	2.145	2.146	45
102	1.982	1.983	3
120	1.8676	1.8677	2
112	1.7239	1.7244	10
121	1.7145	1.7149	30
300	1.6468	1.6472	20
202	1.6283	1.6281	1
220	1.4266	1.4265	15
311	1.3069	1.3066	15
400	1.2353	1.2354	<1
222	1.1914	1.1911	3
401	1.1883	1.1880	5
321	1.0969	1.0967	5

this product were indexed as hexagonal with a = 5.706 and c = 4.329 Å (see Table I), in reasonable agreement with the pattern reported by Arjomand and Machin (*2*) for $BaNiO_{2.36}$. Although $BaNiO_2$ would be expected in the ternary under closed system conditions, these air preparations quenched from 1000°C lead to some excess oxygen in the products. In the case of $BaNiO_{2+x}$, a higher oxide is obtained than that formally expected. Under more reducing conditions, or in a closed system with stoichiometric starting materials, the $BaNiO_{2+x}$ product is likely to be $BaNiO_2$, although this remains to be demonstrated. Products of syntheses carried out in air at 1350°C, and which result in a Ba/Ni = 1 phase, exhibit powder diffraction patterns different from those of either $BaNiO_2$ or $BaNiO_{2.36}$, suggesting that yet another phase may exist in the Ba–Ni–O system.

Syntheses within primary phase fields of Y_2BaNiO_5 and $Y_4Ba_3O_9$ indicate joins to a phase along the BaO–NiO binary with Ba/Ni = 3; however, we have not yet obtained a suitable powder pattern for indexing this phase, apparently due to rapid hydration. No evidence of consistency with the reported structural data on Ba_3NiO_4 (*12*) was obtained.

The X-ray powder data for the Y_2BaNiO_5 phase, as prepared, were indexed in the orthorhombic system with a = 3.7620(2), b = 5.7602(3), and c = 11.3298(6) Å. The general condition for allowed reflections, $h + k + l = 2n$, indicates a body-centered lattice. Iodometric titration showed excess oxidation potential, stoichiometrically consistent with the presence of 1.10 ± 0.10% Ni^{3+} resulting from oxygen nonstoichiometry in a formally divalent nickel phase.

Conditions for Synthesis and Stability of Y_2BaNiO_5

Syntheses of Y_2BaNiO_5 by direct combination of $BaCO_3$, NiO, and Y_2O_3 were attempted at several temperatures between 700 and 1400°C in air. Even at the 700°C, substantial formation of Y_2BaNiO_5 was evident after 48 hr, although complete reaction was only obtained above 1200°C. We believe that the difficulty in achieving complete reaction at lower temperatures is related to slow decomposition of $BaCO_3$. Among the additional phases present in the incompletely reacted products of low temperature syntheses are low temperature Y–Ba–O phases, as expected on the basis of the known Y_2O_3–BaO binary. Therefore, the equilibrium phase diagram for the Y_2O_3–BaO–NiO ternary at temperatures below 1000°C must be somewhat different than that shown in Fig. 1.

In order to identify conditions for preparation of stoichiometric material, we attempted to characterize the $f_{O_2} - T$ dependence of the lower boundary of the stability field of Y_2BaNiO_5. The decomposition boundary was first located at 1300°C by re-

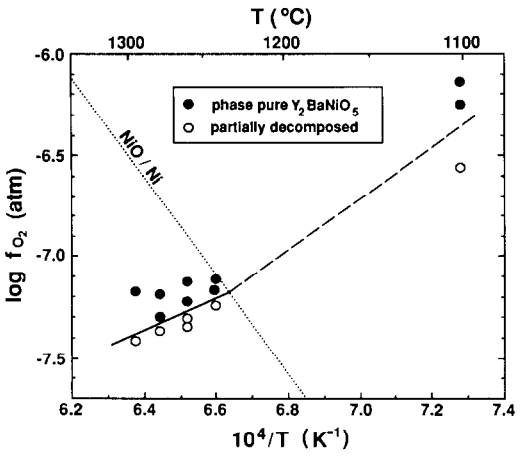

FIG. 2. The temperature dependence of the oxygen fugacity at the decomposition boundary of Y_2BaNiO_5. The NiO/Ni reduction boundary (dotted line) is shown for reference.

peated anneals under increasingly reducing CO_2/CO-buffered atmospheres. Subsequent equilibration at lower temperatures yielded the temperature dependence of the boundary f_{O_2}. Below approximately 1233°C, all CO_2/CO anneals resulted in loss of the Y_2BaNiO_5 phase. It will be shown below that this occurs as a result of reaction with CO_2. To obtain an additional constraint on the boundary at lower temperature, the buffer gas was diluted with Ar to achieve the desired low oxygen fugacity while maintaining a sufficiently low partial pressure of CO_2 to avoid carbonate formation. In all anneals the oxygen fugacity was electrochemically monitored *in situ* with an Y–ZrO_2 cell referenced to 1 atm O_2 and calibrated against the NiO/Ni boundary. The dependence of f_{O_2} on temperature for the boundary reaction is presented in Fig. 2. Solid circles represent anneals with no evidence of decomposition, whereas open circles represent anneals for which decomposition products are observed. Although the decomposition boundary is continuous across the Ni/NiO reduction boundary, the slopes of the Y_2BaNiO_5 boundary dependences on each side of the Ni/NiO boundary differ by a term proportional to the molar free energy of formation of NiO. The temperature dependence of the Y_2BaNiO_5 boundary below the Ni/NiO reduction boundary is approximated by (solid line)

$$\log f_{O_2}\ (\text{atm}) = 7600/T - 12.224$$

which indicates that the reaction is endothermic. There are insufficient data at present to determine the Y_2BaNiO_5 decomposition boundary above the Ni/NiO boundary; however, the dashed line in Figure 2 provides a rough estimate based on the data at 1100°C and the continuity condition at the Ni/NiO boundary. Coexistence of Y_2BaNiO_5 with the decomposition products is observed over a range of oxygen fugacity below the indicated boundary. The products are Y_2O_3, NiO, or Ni^0 (depending on the position relative to the NiO/Ni boundary (Fig. 1)), and a third phase which remains unidentified. From mass balance considerations, the unidentified phase is either a Ba–Ni–O phase with Ba/Ni > 1 or a new Ba-rich Y–Ba–Ni–O phase. The X-ray powder pattern is not consistent with assign-

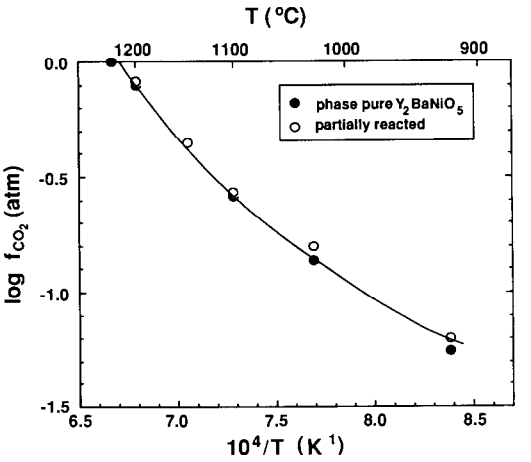

FIG. 3. The temperature dependence of the CO_2 partial pressure for the reaction boundary for carbonate formation from Y_2BaNiO_5.

TABLE II

VARIATION OF LATTICE CONSTANTS AND $\%Ni^{3+}$ WITH ANNEALING CONDITIONS FOR Y_2BaNiO_5

T_a(K)	log f_{O_2}(atm)	$\%Ni^{3+}$	a (Å)	b (Å)	c (Å)	V (Å^3)
1093	0.00	1.78(5)	3.7619(2)	5.7602(3)	11.3319(6)	245.55(5)
1573	0.00	1.10(10)	3.7625(2)	5.7604(3)	11.3290(6)	245.54(5)
1273	−0.68	1.10(10)	3.7620(2)	5.7602(3)	11.3298(6)	245.51(5)
1511	−7.09	0.00(5)	3.7635(2)	5.7604(3)	11.3288(6)	245.60(5)
1374	−6.04	0.00(5)	3.7634(2)	5.7603(3)	11.3288(6)	245.59(5)

ment of the unidentified product as Ba_3NiO_4.

Evidence for reaction of Y_2BaNiO_5 with CO_2 was obtained by fixing the f_{O_2} at 0.10 atm and observing the relationship between partial pressure of CO_2 and temperature at the reaction boundary (see Fig. 3). The reaction is exothermic and appears to have a significantly temperature-dependent enthalpy of reaction, giving rise to the curvature in the boundary (Fig. 3). The reaction products are indistinguishable from those obtained from the boundary reaction in Fig. 2 for oxygen fugacities above the NiO/Ni boundary. The two boundaries differ in that the latter involves direct reaction of Y_2BaNiO_5 with CO_2, whereas the former produces the carbonate indirectly. It is apparent that CO_2/CO or CO_2/H_2 buffers may be used to control oxygen nonstoichiometry only if the CO_2 partial pressure is low enough to avoid direct carbonate formation.

Structure and Stoichiometry in $Y_2BaNiO_{5+\delta}$

X-ray powder diffraction data were collected at room temperature for five Y_2BaNiO_5 samples annealed under various conditions of temperature and oxygen fugacity. A summary of the annealing conditions, $\%Ni^{3+}$, and lattice parameters is provided in Table II. The X-ray powder data for stoichiometric $Y_2BaNiO_{5.000}$ are presented in Table III. All X-ray powder data were collected at room temperature with an internal silicon (NIST) standard.

Single Crystal Growth and Structural Refinement

In order to attempt growth of single crystals from the melt by radio frequency skull melting (*15*), approximately 1450 g of starting material with composition $3Y_2O_3 \cdot 4BaO \cdot 4NiO$ was first prereacted at 1350°C using the procedure described above. The sintered product was then ground and loaded into the water-cooled skull crucible. The composition $3Y_2O_3 \cdot 4BaO \cdot 4NiO$ was chosen in an attempt to segregate crystals of $BaNiO_2$ and the new phase. A graphite susceptor was placed just below the surface of the powder to initiate rf coupling. A 125-liter controlled atmosphere chamber surrounding the crucible was evacuated and refilled with 50% O_2/50% CO_2 to avoid possible reduction of nickel during initiation of the melt. The operating frequency was approximately 2.7 MHz using a Lepel dual frequency generator with a maximum power level of 50 kW. After achieving a stable melt, the atmosphere was changed to 10% O_2/90% CO_2, which is usually suitable for stabilization of divalent nickel oxides at temperatures up to at least 2000°C. The crucible was mechanically lowered with respect to the work coil at a rate of 1.5 cm/hr in order to decouple and grow crystals in a Bridgeman-like fashion.

The boule was found to contain an inti-

TABLE III

X-RAY POWDER DIFFRACTION DATA FOR STOICHIOMETRIC $Y_2BaNiO_{5.000}$ OBTAINED WITH AN INTERNAL SILICON STANDARD USING CuKα RADIATION.

h k l	d_{obsd} (Å)	d_{calcd} (Å)	I/I_0
0 0 2	5.67	5.66	1
0 1 1	5.14	5.13	<1
1 0 1	3.571	3.571	8
0 1 3	3.158	3.158	45
1 1 0	3.150	3.151	2
0 2 0	2.880	2.880	32
0 0 4	2.833	2.832	16
1 1 2	2.753	2.753	100
0 2 2	2.567	2.567	3
1 2 1	2.242	2.242	17
0 1 5	2.108	2.109	3
1 1 4	2.105	2.106	2
0 2 4	2.0198	2.0194	20
1 2 3	1.9564	1.9563	4
1 0 5	1.9412	1.9411	11
0 0 6	1.8879	1.8881	8
2 0 0	1.8821	1.8817	11
0 3 3	1.7118	1.7116	4
1 3 2	1.6374	1.6373	10
1 1 6	1.6195	1.6196	3
2 1 3	1.6162	1.6165	5
1 2 5	1.6099	1.6097	8
0 2 6	1.5791	1.5791	4
2 2 0	1.5752	1.5753	6
2 0 4	1.5673	1.5673	1
0 1 7	1.5582	1.5581	4
2 2 2	1.5178	1.5177	<1
1 0 7	1.4867	1.4868	1
1 3 4	1.4642	1.4641	2
0 4 0	1.4400	1.4401	4
2 2 4	1.3764	1.3767	5
1 4 1	1.3357	1.3356	1
2 0 6	1.3327	1.3328	2
1 1 8	1.2917	1.2916	4
0 4 4	1.2838	1.2837	1
1 3 6	1.2671	1.2676	2
2 3 3	1.2661	1.2661	1
0 3 7	1.2375	1.2375	1
2 2 6	1.2094	1.2096	1
2 1 7	1.1998	1.2001	1
3 1 2	1.1980	1.1980	2
1 0 9	1.1941	1.1938	1
1 4 5	1.1565	1.1566	1
3 2 1	1.1446	1.1442	1
2 4 0	1.1434	1.1436	1
0 0 10	1.1328	1.1329	<1
1 2 9	1.1026	1.1028	<1
0 5 3	1.1015	1.1019	<1
3 0 5	1.0972	1.0975	<1
1 3 8	1.0907	1.0908	1
1 5 2	1.0812	1.0813	1
2 4 4	1.0602	1.0604	<1
0 2 10	1.0542	1.0543	1

Note. Annealing conditions were 1374 K and $\log f_{O_2} = -6.04$.

mate mixture of small crystals of $BaNiO_2$ and Y_2BaNiO_5. In a cavity which formed just beneath the boule surface, a large number of well-formed crystals of the Y–Ba–Ni–O phase had grown, apparently by vapor transport, and many were completely free from $BaNiO_2$. These crystals were optically dense transparent yellow–green with a platey habit consisting of all orthogonal faces and typical dimensions of $1.5 \times 0.2 \times 0.06$ mm^3. Some of the crystals were macroscopically intergrown with black $BaNiO_2$, suggesting that some structural registry exists between phases. Under polarized light the Y–Ba–Ni–O phase exhibits strongly pleochroic behavior, with colors ranging from blue–green to brown, characteristic of a highly anisotropic structure. Many crystals grew together at a characteristic angle suggesting that a twinning law exists.

Several crystals of the Y–Ba–Ni–O phase which appeared free from $BaNiO_{2+x}$ were selected for screening for structure determination by four-circle X-ray diffraction. The crystal chosen for study had dimensions $0.07 \times 0.10 \times 0.26$ mm^3. The lattice constants obtained from 25 high-angle reflections ($35° < 2\theta < 50°$) are $a = 3.7703(6)$, $b = 5.7760(11)$, and $c = 11.3581(23)$ Å. These lattice parameters are larger by 0.25% than those described earlier for powder samples, well outside the limits of error. We have no explanation for this discrepancy at present.

TABLE IV

ATOMIC COORDINATES, ISOTROPIC AND ANISOTROPIC THERMAL PARAMETERS ($\times 10^3$ Å^2), AND SITE SYMMETRIES FOR Y_2BaNiO_5

Atom	Ocupancy	x	y	z	U_{eq}[a]	U_{11}	U_{22}	U_{33}	U_{23}	Site symmetry
Ba	0.125	0	0	0	8(1)	11(1)	6(1)	7(1)	0	*a*
Y	0.250	0	0.5	0.2061(1)	4(1)	6(1)	4(1)	4(1)	0	*j*
Ni	0.125	−0.5	0.5	0	5(1)	4(1)	7(1)	6(1)	0	*c*
O(1)	0.125	0	0.5	0	10(1)	6(2)	17(1)	6(1)	0	*d*
O(2)	0.500	0	0.2394(4)	0.3510(2)	9(1)	9(1)	7(1)	9(1)	3(1)	*l*

[a] One-third of the trace of the orthogonalized U_{ij} tensor. The anisotropic temperature factor exponent takes the form: $-2\pi^2(h^2a^*U_{11} + \ldots 2hka^*b^*U_{12})$. $U_{12} = U_{13} = 0$.

The long axis of the crystal was determined to be [100]. The intensities of 622 reflections in the range $4° < 2\theta < 75°$ and for $-5 < h < 5$, $0 < k < 9$, and $0 < l < 18$ (two forms) were measured at 295 K. Systematic absences confirm an *I*-centered lattice, with possible space groups *Immm* (71), *I*222 (23), *Imm*2 (44),and $I2_12_12_1$ (24) (*16*). An analytical correction for absorption (μ = 357.41 cm^{-1}) was applied to the data, and the two forms merged (R_{int} = 3.4%) to yield 369 independent, observed data with $F_0 \geq 3\sigma(F_0)$; 38 data were rejected as unobserved. Using a three-dimensional Patterson map, the Ba sites were first located, followed by Y and Ni. Oxygen positions were obtained from a difference Fourier map. The formula unit was determined to be Y_2BaNiO_5 with Z = 2. The centrosymmetric space group *Immm* was chosen giving a final refinement with R_F = 0.0257 and R_{wF} = 0.0281 using anisotropic thermal factors (Table IV). No trends or systematic errors in F or significant residual electron density were observed ($\Delta\rho_{max}$ = 1.7 eÅ^3). All computations and sources of neutral atom scattering factors are contained in the SHELXTL program library (Version 5.1, G. Sheldrick, Nicolet XRD, Madison, WI).

Y_2BaNiO_5 is isomorphous with the structures of Nd_2BaNiO_5 (*17*), Dy_2BaNiO_5 (*18*), and $GdBaNiO_5$ (*19*). The atomic coordinates, site symmetries, and anisotropic thermal parameters are presented in Table IV. Table V lists interatomic distances and angles. A clinographic projection of the structure viewed along (100) is presented

TABLE V

INTERATOMIC BOND DISTANCES AND ANGLES FOR Y_2BaNiO_5

Interatomic separations (Å)			Interatomic angles (°)	
Ba–O(2)	2.947(2)	8	O(2)–Ba–O(2)	61.4(1)
Ba–O(1)	2.888(1)	2	O(2)–Ba–O(2)	70.1(1)
Ni–O(2)	2.186(2)	4	O(2)–Ba–O(2)	79.5(1)
Ni–O(1)	1.8847(4)	2	O(2)–Ba–O(2)	100.5(1)
Y–O(2a)	2.259(2)	2	O(2)–Ba–O(2)	109.9(1)
Y–O(2b)	2.416(2)	4	O(2)–Ba–O(2)	118.6(1)
Y–O(1)	2.302(1)	1	O(2)–Ba–O(2)	180.0
Ba–Ni	3.449(1)	4	O(2)–Ba–O(1)	59.3(1)
Ba–Y	3.693(1)	4	O(2)–Ba–O(1)	120.7(1)
Ba–Y	3.868(1)	4	O(2)–Ni–O(2)	78.5(1)
Ni–Y	2.975(1)	4	O(2)–Ni–O(2)	101.5(1)
Ba–Ba	3.7703(6)	2	O(2)–Ni–O(2)	180.0
Ni–Ni	3.7703(6)	2	O(2)–Ni–O(1)	90.0
Y–Y	3.770(1)	2	O(1)–Ni–O(1)	180.0
Y–Y	3.613(1)	4	O(2)–Y–O(2)	69.8(1)
O(2)–O(2)	2.765(3)	1	O(2)–Y–O(2)	78.8(1)
O(2)–O(2)	2.971(3)	4	O(2)–Y–O(2)	78.9(1)
O(2)–O(2)	3.011(3)	1	O(2)–Y–O(2)	102.6(1)
O(2)–O(2)	3.7703(6)	2	O(2)–Y–O(2)	124.7(1)
O(2)–O(2)	3.385(4)	1	O(2)–Y–O(2)	150.8(1)
O(1)–O(1)	3.7703(6)	2	O(2)–Y–O(1)	75.4(1)
O(2)–O(1)	2.886(3)	8	O(2)–Y–O(1)	138.2(1)

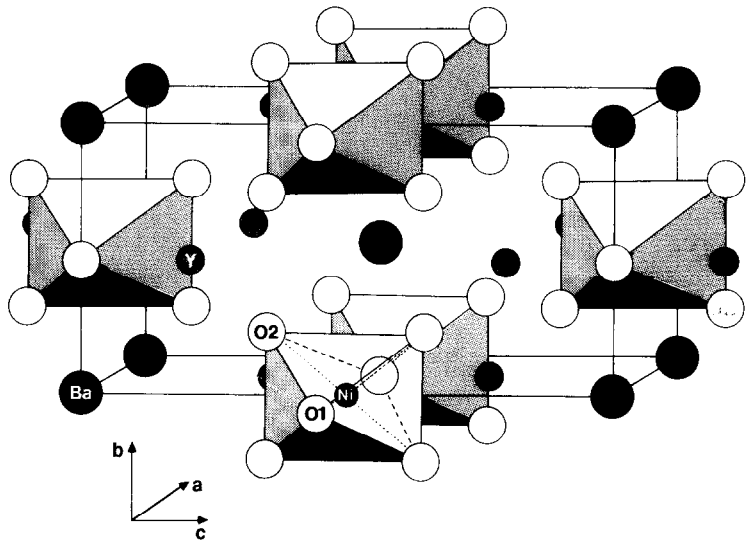

FIG. 4. A clinographic projection of the Y_2BaNiO_5 structure viewed along (001).

in Fig. 4. The most striking feature of this structure is the presence of isolated chains of highly compressed corner-shared NiO_6 octahedra. The yttrium site is coordinated by seven oxygen atoms in a capped trigonal prism as shown in Fig. 5a. The barium site is a 10-coordinate bicapped quadrangular prism as shown in Fig. 5b.

Discussion

The phase diagram shows general agreement with the literature reports for each of the binary oxide systems. As expected, no additional phases were observed along the Y_2O_3–NiO binary. The presence of two stable phases along the Y_2O_3–BaO binary is

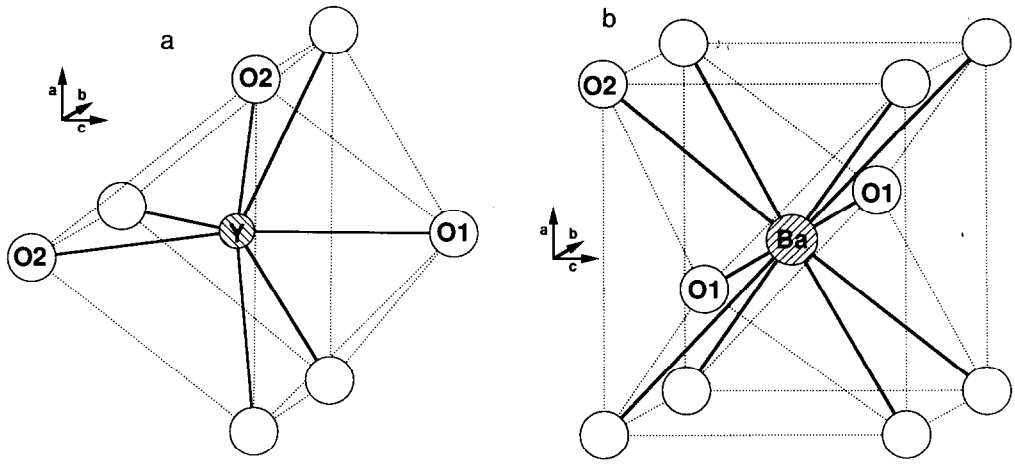

FIG. 5. Local coordination environments for (a) the Y site and (b) the Ba site. Note that the spatial orientations are rotated from those in Fig. 4. Refer to Table IV for the associated interatomic separations.

also expected for the temperature range of this investigation, as previous reports indicate that only $Y_4Ba_3O_9$ and Y_2BaO_4 exist above 1200°C. These two phases are formed at 1350°C, and do not decompose upon cooling to 1000°C. The other two compounds reported to exist along the binary, $Y_2Ba_4O_7$ and $Y_2Ba_2O_5$, were also observed in preparations at lower temperatures. Identification of the two additional phases along the BaO–NiO binary was difficult due to problems with melting and/or reaction with the crucible materials, increased nickel oxidation state due to use of the ambient atmosphere, and because of hydration. X-ray powder diffraction patterns of samples prepared at 1000°C are consistent with the previously reported data for $BaNiO_{2.36}$, a higher oxide than the expected $BaNiO_2$. Constraints on Alkemade joins indicate that a phase with composition Ba_3NiO_{4+x} is present, rather than strictly divalent Ba_3NiO_4. If additional care is taken to prevent exposure of products to moisture and CO_2, and if a somewhat more reducing atmosphere is provided to avoid mixing 2+/3+ oxides of nickel, it appears that the phases $BaNiO_2$ and Ba_3NiO_4 should be observed.

The decomposition boundary of the new phase, Y_2BaNiO_5, at low oxygen fugacity appears not to be a simple reduction boundary. Since strictly divalent nickel phases are observed on both sides of the Y_2BaNiO_5 boundary for conditions on the NiO side of the NiO/Ni boundary, the dependence of the former boundary reaction on f_{O_2} must be implicit. The individual free energies of formation of the product and reactant oxides in the boundary reaction each have distinct functional f_{O_2}-T dependences, and therefore must result in dependence of the boundary reaction on f_{O_2} and temperature. Although the free energies of formation of the products NiO and Y_2O_3 are known, as is ΔG^{rxn}, the free energy of formation of Y_2BaNiO_5 cannot be determined without information on the third decomposition product. This unknown product cannot be BaO, which would form $BaCO_3$ in the presence of CO_2 in the buffer gas, since (i) the X-ray powder data do not support this and (ii) the Alkemade triangle cannot be closed with $Y_4Ba_3O_9$ and Y_2BaO_4 present along the Y_2O_3–BaO binary. In principle, given more detailed decomposition boundary data, it should be possible to estimate the Ba/Ni ratio of the unknown carbonate by mass balance by first determining the stoichiometric coefficient of NiO from the relative van't Hoff slopes on either side of the Ni/NiO boundary.

The dependence of lattice parameters of Y_2BaNiO_5 on oxygen nonstoichiometry seems to be small, as is the range of nonstoichiometry observed. A slight decrease in a is evident as the trivalent nickel content increases, reflecting a small decrease in the Ni–O bond distance. Along the chain axis, which is parallel to (100), the Ni–O bond distance is a remarkably short 1.88 Å, while the four equivalent bond lengths orthogonal to the chain axis are 2.19 Å. This distortion is the inverse of the 4 + 2 distortion observed in the layered perovskite nickelates in which the apical oxygen bond lengths are typically elongated by about 14% with respect to the basal oxygen bond lengths. In the present case the octahedral axial compression amounts to 14%. These lower-dimensional, corner-shared structural families both possess highly compressed covalent transition metal oxygen interactions in one and two dimensions, respectively. Thus, Y_2BaNiO_5 and lanthanide counterpart may be expected to exhibit strongly anisotropic physical properties. Characterization of the magnetic properties of Y_2BaNiO_5 is currently in progress.

Effective Radii and Coordination Numbers

To further investigate the nature of coordination environments in Y_2BaNiO_5, the method of Fink and Hoppe (*20*) for obtaining

mean effective ionic radii ($\underline{R}^*_M$) and effective coordination number (C_{eff}) will be considered. Effective ionic radii are first obtained as a fraction of the interatomic distance from a metal atom of interest, M, to the neighboring oxygens, O_i, in the coordination environment.

$$R^*_{MO_i} = R_{obsdMO_i} \cdot f_{MO},$$

where R_{obsdMO_i} is the observed separation between M^{n+} and O_i^{2-}, and $R^*_{MO_i}$ is the fraction of that separation attributed to M^{n+}. The quantity f_{MO} is obtained from tabulated data on ionic radii for the appropriate coordination environment as

$$f_{MO} = I_{M^{n+}}/(I_{M^{n+}} + I_{O^{2-}}).$$

The mean effective ionic radius is given by

$$\underline{R}^*_M = \frac{\Sigma n_{MO_i} R^*_{MO_i} \exp[1 - (R^*_{MO_i}/R^*_{MO_i\min})^6]}{\Sigma n_{MO_i} \exp[1 - (R^*_{MO_i}/R^*_{MO\min})^6]},$$

where n_{MO_i} is the number of equivalent M–O_i distances and $R^*_{MO_{min}}$ is the smallest M–O separation in the set. The exponential term is a dispersion factor which is similar to a Lennard–Jones function and gives reliable weighting in well-characterized cases such as close-packed structures. The effective coordination number is defined as

$$C_{eff} = \Sigma n_{MO_i} \exp[1 - (R^*_{MO_i}/\underline{R}^*_M)^6].$$

Using the structural data presented above for Y_2BaNiO_5, along with the structural refinement data for Gd_2BaNiO_5 (*19*), La_2NiO_4 (*21*), and Pr_2NiO_4 (*22*), $\underline{R}^*_M$ and C_{eff} values were calculated. Ionic radii were obtained from tabulations by Shannon (*23*). Results for metal sites in Y_2BaNiO_5 and Gd_2BaNiO_5 are compared with the layered perovskite nickelates La_2NiO_4 and Pr_2NiO_4 in Table VI. It is apparent that the site characteristics in the linear chain phases are very similar. By comparison with layered perovskites of nickel for which the nickel $C_{eff} \approx 5$, the C_{eff} of nickel in these one-dimensional phases is unusually low at 4.4. The mean effective ionic radii values for divalent nickel are somewhat smaller in the linear chain structures than those of the layered perovskites. Although the effective radius for Y^{3+} is smaller than Gd^{3+}, the coordination numbers are remarkably similar. By comparison, the A site (La,Pr) effective coordination number in the layered perovskites seems much less consistent, perhaps suggesting a greater tolerance for site identities and coordination environments. The Ba sites in the linear chain phases show a consistent effective radius, and minor variation in effective coordination from the expected $C_{eff} = 10$ for a nearly uniform 10-fold coordinate environment typical of Ba.

TABLE VI

MEAN EFFECTIVE IONIC RADII (MEIR) AND EFFECTIVE COORDINATION NUMBERS (ECoN) FOR METAL SITES IN Y_2BaNiO_5, Gd_2BaNiO_5, La_2NiO_4, AND Pr_2NiO_4

Composition	Metal site	$\underline{R}^*_M$	C_{eff}
Y_2BaNiO_5	Y	0.943	6.72
	Ba	1.478	9.97
	Ni	0.680	4.39
Gd_2BaNiO_5	Gd	0.985	6.76
	Ba	1.485	9.55
	Ni	0.684	4.39
La_2NiO_4	La	1.178	6.92
	Ni	0.654	5.09
Pr_2NiO_4	Pr	1.129	6.14
	Ni	0.651	5.18

Acknowledgments

Funding for this investigation was provided by the University of Delaware Research Foundation (UDRF). The authors thank Professor J. M. Honig for making the rf induction skull melting facility at Purdue University available to us for the growth of the single crystals used in this investigation.

References

1. E. N. TIMOFEEVA, N. I. TIMOFEEVA, L. N. DROZDOVA, AND O. A. MORDOVIN, *Izv. Akad. Nauk SSSR, Neorg. Mater.* 3, 187 (1967).

2. M. ARJOMAND AND D. J. MACHIN, *J. Chem. Soc., Dalton Trans.* 1055, (1975).
3. H. K. MULLER-BUSCHBAUM, *Naturwissenschaften* **51,** 508 (1964).
4. I. M. MAISTER AND L. M. LOPATO, *Izv. Akad. Nauk, SSSR, Neorg. Mater.* **9,** 64 (1973).
5. L. M. LOPATO, I. M. MAISTER, AND A. V. SHENCHENKO, *Izv. Akad. Nauk. SSSR, Neorg. Mater.* **8,** 861 (1972).
6. W. KWESTROO, H. A. M. VAN HAL, AND C. LANGEREIS, *Mater. Res. Bull.* **9,** 1631 (1974).
7. L. KOVBA, L. N. LYKOVA, AND E. V. ANTIPOV, *Russ. J. Inorg. Chem. (Engl. Transl.)* **28,** 409 (1983).
8. W. WONG-NG, H. MCMURDIE, B. PARETZKIN, C. HUBBARD, AND A. DRAGOO, *Powder Diffract. J.* **38,** 1377 (1987).
9. J. J. LANDER, *J. Amer. Chem. Soc.* **73,** 2450 (1951).
10. J. J. LANDER, *Acta Crystallogr.* **4,** 148 (1951).
11. H. KRISCHNER, K. TORKAR, AND B. O. KOLBESEN, *J. Solid State Chem.* **3,** 349 (1971).
12. J. J. LANDER AND L. A. WOOTEN, *J. Amer. Chem. Soc.* **73,** 2452 (1951).
13. Y. TAKEDA, F. KANAMARU, M. SHIMADA, AND M. KOIZUMI, *Acta Crystallogr., Sect. B* **32,** 2464 (1976).
14. M. SHIMADA, Y. TAKEDA, H. TAGUCHI, F. KANAMARU, AND M. KOIZUMI, *J. Cryst. Growth* **29,** 75 (1975).
15. D. J. BUTTREY, H. R. HARRISON, J. M. HONIG, AND R. R. SCHARTMAN, *J. Solid State Chem.* **54,** 407 (1984).
16. "International Tables for Crystallography," Vol. A, Reidel, Dordrecht, (1987).
17. ST. SCHIFFLER AND HK. MÜLLER-BUSCHBAUM, *Z. Anorg. Allg. Chem.* **532,** 10 (1986).
18. HK. MÜLLER-BUSCHBAUM AND I. RÜTER, *Z. Anorg. Allg. Chem.* **572,** 181 (1989).
19. J. AMADOR, E.GUTIERREZ PUEBLA, M. A. MONGE, I. RASINES, J. A. CAMPA, J. M. GOMEZ DE SALAZAR, AND C. RUIZ VALERO, *Solid State Ionics* **32/33,** 123 (1989).
20. D. FINK AND R. HOPPE, *Z. Anorg. Allg. Chem.* **422,** 1 (1976).
21. D. J. BUTTREY AND A. L. RHEINGOLD, IN PREPARATION.
22. D. J. BUTTREY, J. D. SULLIVAN, AND A. L. RHEINGOLD, in preparation.
23. R. D. SHANNON, *Acta Crystallogr., Sect. A* **32,** 751 (1976).